Electronic Supplementary Material (ESI) for Journal of Materials Chemistry A

Engineering electronic band structure of ternary thermoelectric nanocatalysts for highly efficient detection of hydrogen sulfide

Hongyuan Shang[a, b1*], Xiaofei Zhang[b1], Aiping Zhang[b*], Jinwen Du[c*] and Ruiping Zhang[d*]

[a]*Department of Radiology, Third Hospital of Shanxi Medical University, Shanxi Bethune Hospital, Taiyuan 030032, China*

[b]*College of Pharmacy, Shanxi Medical University, Taiyuan 030001, PR China*

[c]*Stomatological Department, Taiyuan Municipal No.2 People's Hospital, Taiyuan 030002, China*

[d]*The Radiology Department of Shanxi Provincial People's Hospital, The Fifth Hospital of Shanxi Medical University, Taiyuan, 030001, China*

[*]Corresponding author: Aiping Zhang (A. Zhang); Jinwen Du (J. Du); Ruiping Zhang (R. Zhang)

E-mail: shanghongyuan@sxmu.edu.cn; zhangap1@163.com;

Djw734600519@163.com; zrp_7142@sxmu.edu.cn

[1]Hongyuan Shang and Xiaofei Zhang contributed equally to this paper.

1. Experimental Section

1.1 Materials and instruments

Potassium tellurite (K_2TeO_3, 90%), platinum (II) acetylacetonate ($Pt(acac)_2$, 97%), L-ascorbic acid (AA,99%), polyvinylpyrrolidone (PVP, K29-32), ethylene glycol (EG, 98%), copper chloride ($CuCl_2$, 98%), 3, 3′, 5, 5′-tetramethylbenzidine (TMB, 98%), sodium sulfide nonahydrate ($Na_2S·9H_2O$, 98%) were purchased from Aladdin (Shanghai, China). All chemicals in this experiment were of analytical purity without require additional purification.

Morphology of the prepared product was characterized by Transmission electron microscopy scanning (TEM) of HITACHI HT7700 (acceleration voltage :120 kV). Powder X-ray Diffraction (PXRD) patterns were collected by X'Pert-Pro MPD diffractometer of Netherlands PANalytical with a Cu Kα X-ray source (λ = 1.540598 Å). X-ray photoelectron spectroscopy (XPS) was conducted with an SSI S-Probe XPS Spectrometer. Fourier transform infrared spectroscopy (FT-IR) spectra were collected on a Bruker Vertex 80v vacuum FTIR spectrometer. The absorbance spectra were acquired on an ultraviolet and visible spectrophotometer (UV-2550, Shimadzu, Japan).

1.2 Synthesis of PtTeCu NRs

PtTe NRs were first prepared according to the reported literature. Briefly, 25.6 mg of potassium tellurite (K_2TeO_3), 20 mg of platinum (II) acetylacetonate ($Pt(acac)_2$, 71.2 mg of L-ascorbic acid (AA), 200 mg of polyvinylpyrrolidone (PVP), 10 mL of ethylene glycol (EG), and 10 mL of water were mixed into a 30 mL of glass bottle and then ultrasonicated for 1.5 h. After that, the glass bottle was transferred to a Teflon-lined stainless-steel autoclave and heated at 180℃ for 5 h in an oven. For the preparation of PtTeCu NRs, 2.8 mg of copper chloride ($CuCl_2$) were dispersed in 6 mL of EG. The above EG solution of $CuCl_2$ was poured into the EG solution of PtTe NRs to heat at 180℃ for 3 h in an oil bath. Finally, the product was obtained by centrifugation and washed with an ethanol/acetone (v/v 1:9) mixture.

1.3 Examining Peroxidase-Like Catalytic Activities of PtTeCu NRs

Peroxidase-like activity: The peroxidase-mimicking activity was investigated by utilizing TMB as chromogenic substrate at room temperature under a weak acidic

condition (pH 5.0, 0.1 M PBS buffer solution). The absorbance signal of oxTMB was recorded at 652 nm via UV-Vis spectrophotometer. In detail, 20 μL of PtTeCu NRs aqueous solution (1 mg·mL^{-1}), 120 μL of H_2O_2 solution (1 mM), and 480 μL of TMB solution (1 mM) were sequentially added into 0.1 M PBS solution (pH 5.0). The final volume was fixed to 3.0 mL by adding PBS solution (pH 5.0). After 10 min, the catalytic oxidation of TMB was detected by their UV-Vis absorption spectra.

Enzymatic kinetic analysis: Further kinetic assay was conducted for TMB oxidation at different concentrations of H_2O_2 solution by utilizing PtTeCu NRs. The experiment conditions were similar to that of peroxidase-like activity, in which 250 μL of 0.1 M PBS solution (pH 5.0) containing 3 μL of PtTeCu NRs (0.5 mg·mL^{-1}) aqueous solution, 20 μL of TMB solution and different volumes of H_2O_2 solution (0.5, 1, 5, 10, 20 and 40 mM). The kinetic constants (K_m and V_{max}) were obtained according to Michaeli-Menten equation:

$$V_0 = \frac{V_{max}[S]}{K_m + [S]} \quad (1)$$

where V_0 represents the initial velocity, [S] stands for the concentration of the substrate, K_m represents the Michaelis-Menten constant, and V_{max} represents the maximal reaction velocity. The value of K_m was equivalent to the substrate concentration at which the rate of conversion was half of V_{max}.

The optimization of experimental condition: To evaluate the activity of PtTeCu NRs to PtTeCu NRs concentration, and pH value, their peroxidase-like activities were detected at various PtTeCu NRs concentrations (1, 2, 3, 6, 8, and 10 μg·mL^{-1}), or buffer soution with various pH values (4.5, 5.0, 5.5, 6.0, 7.0, and 8.0).

1.4 Examining Photothermal Effect of PtTeCu NRs

Aqueous solutions containing different concentrations of PtTeCu NRs (100, and 200 μg·mL^{-1}) were exposed to 808 nm laser (1.0 W·cm^{-2}) for 8 min. And the temperature changes were recorded by an infrared camera. The temperature change of different concentrations PtTeCu NRs solution (25, 50, 100, 200, and 500 μg·mL^{-1}) under 808 nm laser power intensities (1.0 W·cm^{-2}) was recorded. To further evaluate the photothermal stability of PtTeCu NRs, PtTeCu NRs solution (100 μg·mL^{-1}) was irradiated by an 808

nm laser at 1.0 W·cm^{-2} during the heating and cooling processes for three cycles. The photothermal conversion efficiency (η) was calculated as follows:

$$\eta = \frac{hS(T_{max} - T_{surr}) - Q_{dis}}{I(1 - 10^{-A808})} \quad (2)$$

where S (cm^2) refers to the surface area of the container; η (W·cm^{-2}·K^{-1}) is the heat transfer coefficient; T_{max} (K) is the equilibrium temperature; T_{surr} is the surrounding ambient temperature; Q_{dis} (W) represents the heat loss due to absorption by the container which is negligible; I (W·cm^{-2}) is power intensity of the incident laser. A_{808} means the absorbance of the PtTeCu NRs at 808 nm. In addition, hS is calculated using

$$hS = \frac{m_D c_D}{\tau_s} \quad (3)$$

where τ_s represents the time constant of the sample system; m_D and c_D are the mass and heat capacity (4.2 J·g^{-1}·°C^{-1}) of DI water. τ_s is calculated from equations (4, 5):

$$\tau_s = -\frac{\ln\theta}{t} \quad (4)$$

$$\theta = \frac{T - T_{surr}}{T_{max} - T_{surr}} \quad (5)$$

where t is irradiation time; θ means the driving force temperature.

1.5 Pyro-Electrochemical Measurement

The time-dependent pyroelectric current and potential, electrochemical impedance spectroscopy Nyquist plots, and Mott-Schottky curves were recorded on an electrochemical workstation (CHi660e, Shanghai, China) connected with a standard three-electrode system (Calomel reference electrode and graphite counter electrode) placed in the electrolytic cell. The PtTeCu NRs modified glassy carbon electrode was choosen as the working electrode. The electrolyte solution was Na_2SO_4 solution (0.1 M). Ultimately, the working electrode was stimulated under 808 nm laser irradiation for the measurement of electrochemical impedance, pyroelectric current, and potential.

1.6 Analysis of H_2S in 10% FBS

To explore the feasibility of the proposed protocols in the actual application, the 10% FBS was utilized as a real sample. Then, the 10% FBS was filtered and diluted with the 0.1 M PBS (pH 5.0) prior to this detection. Afterward, the diluted samples were spiked with the H_2S solution at distinct levels, and the detailed processes of the analysis test was similar to these for the determination of H_2S.

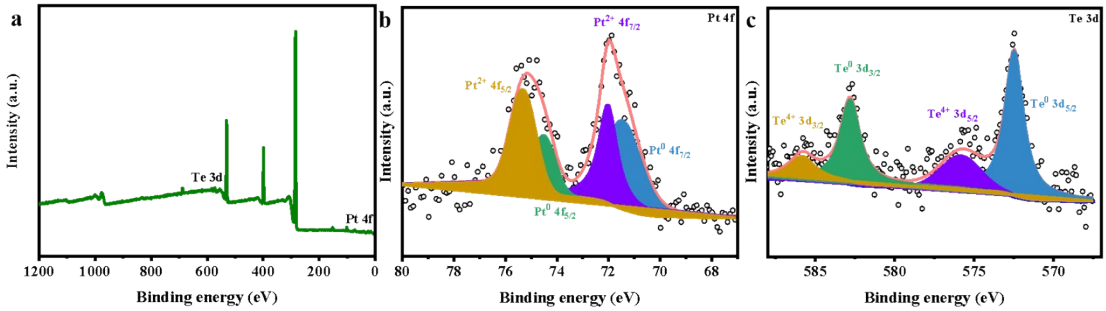

Fig. S1 (a) XPS survey, high-resolution XPS spectra of (b) Pt 4f, and (c) Te 3d in PtTe NRs.

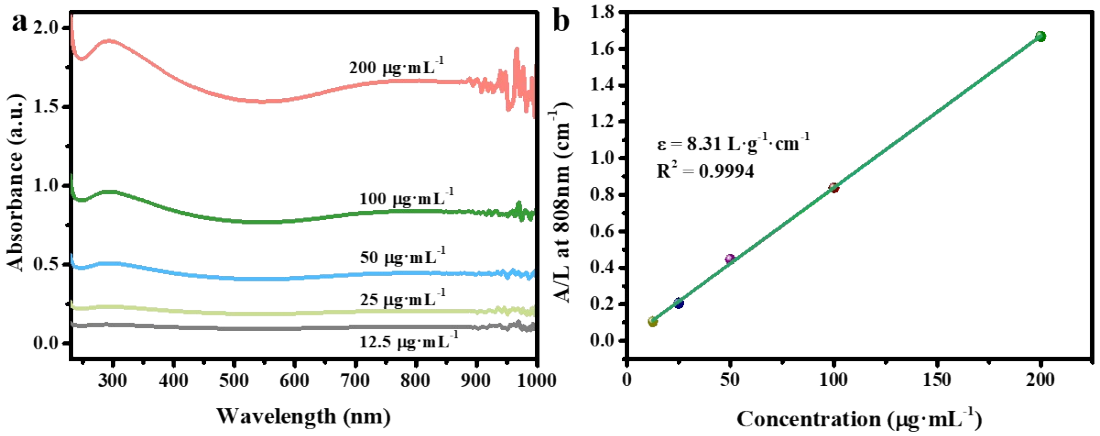

Fig. S2 (a) UV-Vis-NIR absorbance spectra of the PtTeCu NRs with different concentrations (12.5, 25, 50, 100, and 200 μg·mL^{-1}). (b) The fitting curve of the mass extinction coefficient of PtTeCu NRs at 808 nm.

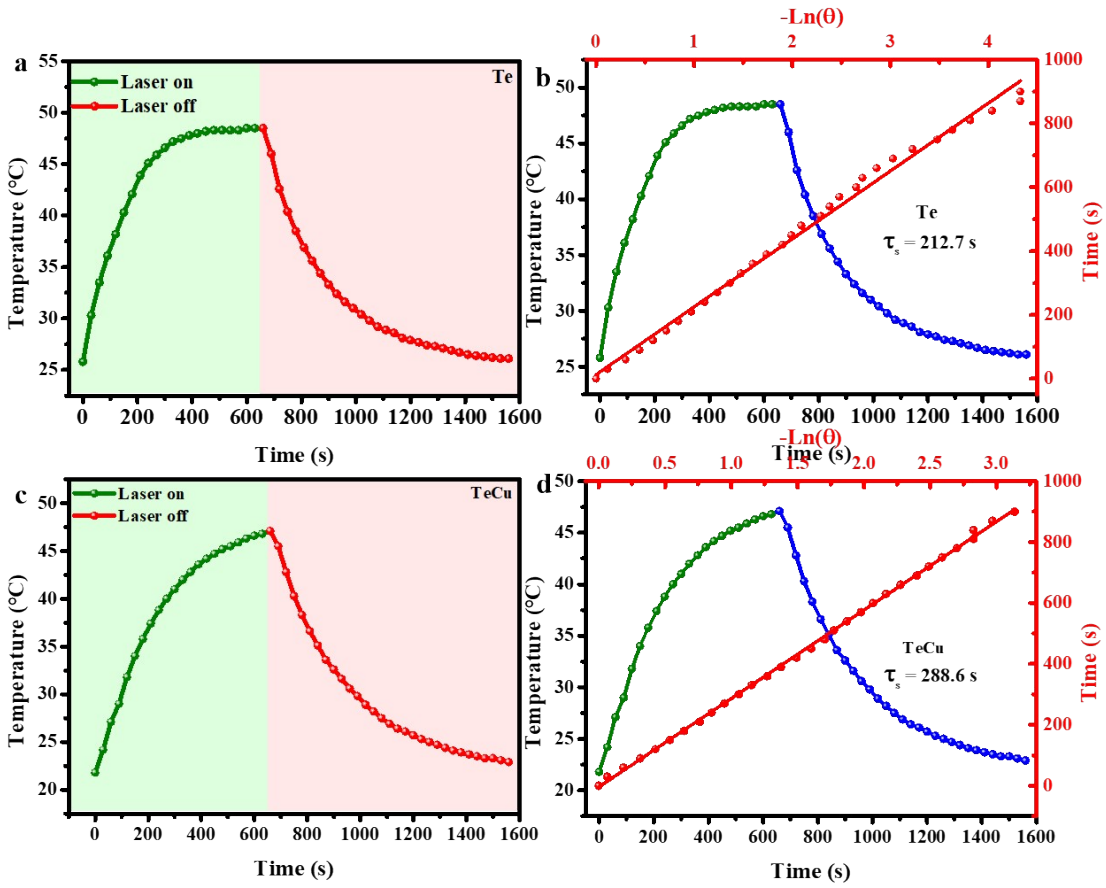

Fig. S3 (a) Heating/cooling curves of Te (b) along with the linear time data obtained from the cooling period. (c) Heating/cooling curves of TeCu (d) along with the linear time data obtained from the cooling period.

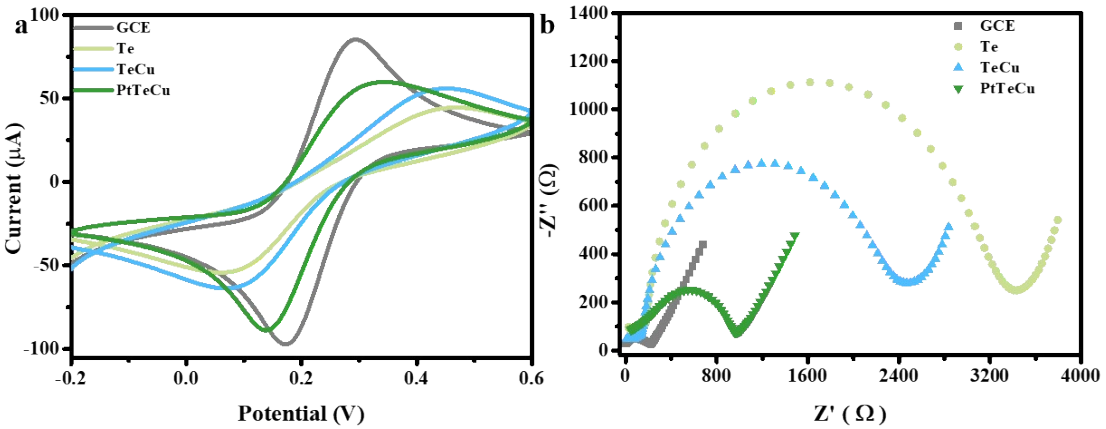

Fig. S4 (a) CV curves and (b) EIS spectra of the different martials modified electrode in 0.1 M KCl including 5 mM $Fe(CN)_6^{3-/4-}$.

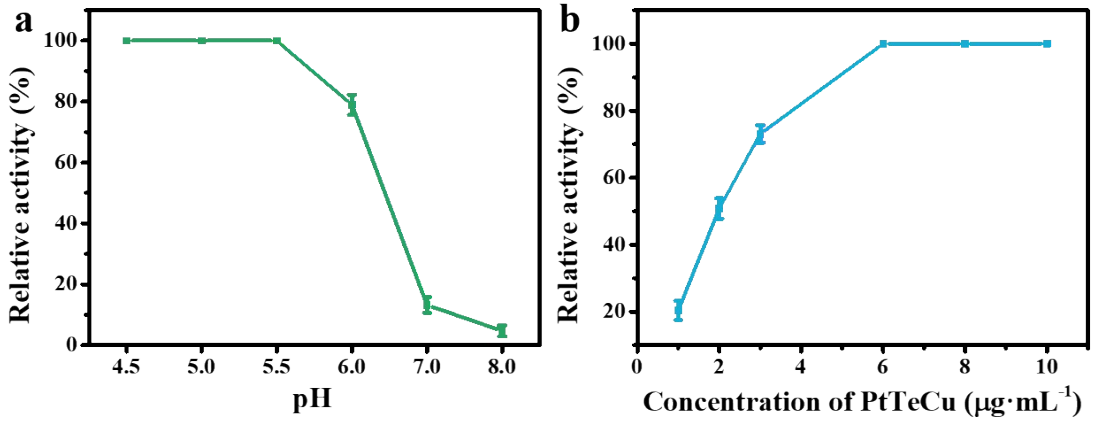

Fig. S5 The optimization of the experimental conditions, including (a) the PBS buffer pH value, (b) the concentration of PtTeCu.

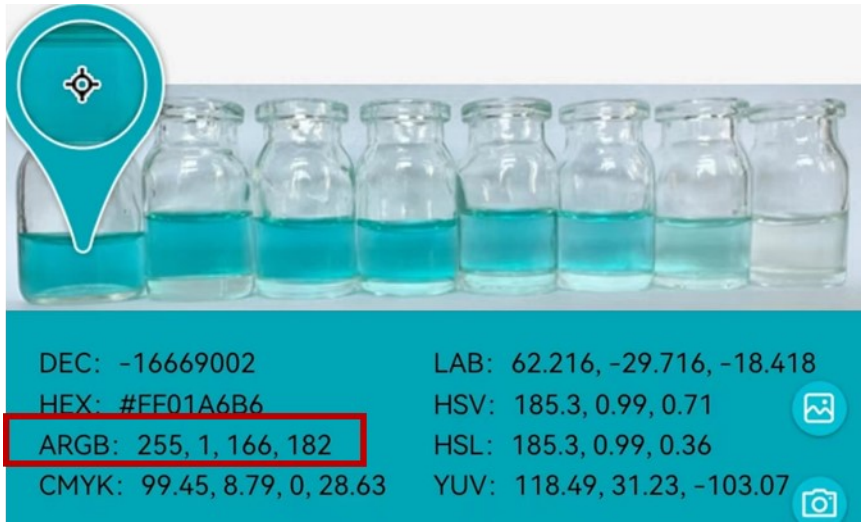

Fig. S6 Smartphone sensing platform according to "Color Selector" APP software for H_2S detection.

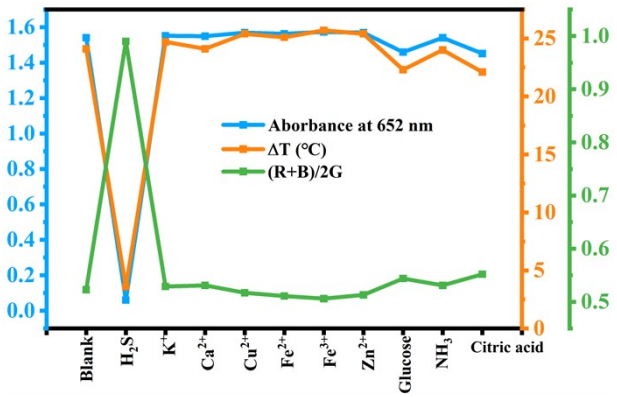

Fig. S7 (a) Absorbance, temperature and smartphone collected of the PtTeCu-based assay in the presence of diverse interference substances (500 μM).

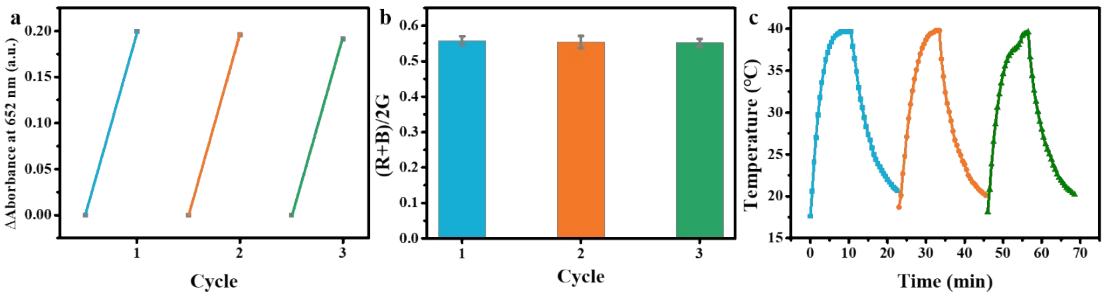

Fig. S8 (a) Absorbance change and (b) color intensity of the reaction system upon cycle addition with H_2S using the PtTeCu-based assay. (c) Thermal cycle stability of the PtTeCu-TMB-H_2O_2-H_2S system.

Table S1 Comparing the detection performance of different methods for H_2S sensing.

Materials	**Analytical methods**	**Linear range (μM)**	**Limit of detection (μM)**	**References**
Cytosine-Ag^+-cytosine	Colorimetry Fluorescence	0.5 - 40 0.5 - 20	2.17 2.5	[1]
BDP	Photoacoustic Imaging	0 - 100	0.59	[2]
Palladium Coordination Polymers	Photothermal	0 - 50	0.79	[3]
Cy7-Cl	Luminescence	1 - 90	0.51	[4]
BFPP	Fluorescence	0.05 - 4	0.017	[5]
SXR	Colorimetry Fluorescence	10 - 80	0.7	[6]
PDMS@MWCNT	Electrochemistry	0.5 - 5	0.005	[7]
PPF-Ag NPs	Colorimetry	0.7 - 10	0.2	[8]
NT-SH	Fluorescence	0.08 - 50	0.08	[9]
Al-MIL-53-N_3	Fluorescence	0.2 - 1.7	0.09	[10]
PtTeCu	Colorimetry	0.5 - 100	0.42	This work

	Photothermal	1 - 100	0.73
	Smartphone	3 - 100	1.41

BDP: Aza-BODIPY derivative

Cy7-Cl: cationic near-infrared cyanine chromophores

BFPP: Self-assembly method assisted by FPP, PEG-PLA, and angiopep2-PEG-PLA

Table S2 H_2S detection in 10% FBS samples by the PtTeCu platform via triple-mode sensing platform (n=3).

Mode	Added (μM)	Found (μM)	Recovery (%)
Colorimetry	10	9.87	98.7
	50	50.3	103.0
Photothermal	10	9.5	95.0
	50	48.5	98.5
Smartphone	10	10.5	104.7
	50	50.1	101.0

References

[1] Q. Liu, Y. Liu, Q. Wan, Q.R. Lu, J. Liu, Y.G. Ren, J.C. Tang, Q. Su, Y.P. Luo, Label-free, reusable, equipment-free, and visual detection of hydrogen sulfide using a colorimetric and fluorescent dual-mode sensing platform, Anal. Chem. 95(14) (2023) 5920-5926.

[2] R.R. Wu, Z.X. Chen, H.Q. Huo, L.L. Chen, L.C. Su, X. Zhang, Y. Wu, Z.C. Yao, S.G. Xiao, W. Du, J.B. Song, Ratiometric detection of H_2S in liver injury by activated two-wavelength photoacoustic imaging, Anal. Chem. 94(30) (2022) 10797-10804.

[3] S.S. He, J. Hai, S.H. Sun, S.Y. Lu, B.D. Wang, Palladium coordination polymers nanosheets: new strategy for sensitive photothermal detection of H_2S, Anal. Chem. 91(16) (2019) 10823-10829.

[4] F.F. Wang, C.L. Zhang, X.T. Qu, S.S. Cheng, Y.Z. Xian, Cationic cyanine chromophore-assembled upconversion nanoparticles for sensing and imaging H_2S in

living cells and zebrafish, Biosens. Bioelectron. 126 (2019) 96-101.

[5] J.B. Li, Y. Zhou, L.F. Song, S. Yang, Q.Q. Wang, Y.B. Zhou, X.B. Zhang, Z.H. Qing, R.H. Yang, Brain-targeted near-infrared nanobeacon for in situ monitoring H_2S fluctuation during epileptic seizures, Anal. Chem. 94(43) (2022) 15085-15092.

[6] X.R. Song, Y.Z. Wang, J.X. Ru, Y. Yang, Y. Feng, C. Cao, K. Wang, G.L. Zhang, W.S. Liu, A mitochondrial-targeted red fluorescent probe for detecting endogenous H_2S in cells with high selectivity and development of a visual paper-based sensing platform, Sens Actuators B Chem. 312 (2020) 127982.

[7] Z.H. Wang, X. Jin, W.Q. Guo, H.W. Liu, T. Yang, H. Zeng, X.L. Luo, An indirect detection strategy-assisted self-cleaning electrochemical platform for in-situ and pretreatment-free detection of endogenous H_2S from sulfate-reducing bacteria (SRB), J. Hazard. Mater. 436 (2022) 129296.

[8] Y. Zhang, H.Y. Shen, X. Hai, X.W. Chen, J.H. Wang, Polyhedral oligomeric silsesquioxane polymer-caged silver nanoparticle as a smart colorimetric probe for the detection of hydrogen sulfide, Anal. Chem. 89(2) (2017) 1346-1352.

[9] Q. Sun, H. Liu, Y. Qiu, J. Chen, F.S. Wu, X.G. Luo, D.W. Wang, A highly sensitive and selective fluorescence turn-on probe for the sensing of H_2S in vitro and in vivo, Spectrochim. Acta A 254 (2021) 119620.

[10] A. Das, S. Banesh, V. Trivedi, S. Biswas, Extraordinary sensitivity for H_2S and Fe(III) sensing in aqueous medium by Al-MIL-53-N_3 metal-organic framework: in vitro and in vivo applications of H_2S sensing, Dalton. T. 47(8) (2018) 2690-2700.